HEFAT2014
10th International Conference on Heat Transfer, Fluid Mechanics and Thermodynamics
14 – 16 July 2014
Orlando, Florida

OPTIMISATION OF AN OPEN RECTANGULAR CAVITY RECEIVER AND RECUPERATOR USED IN A SMALL-SCALE SOLAR THERMAL BRAYTON CYCLE WITH THERMAL LOSSES

Le Roux W.G.[a]*, Bello-Ochende, T.[b] and Meyer J.P.[a]
[a]Department of Mechanical and Aeronautical Engineering, University of Pretoria,
Private Bag X20 Hatfield, Pretoria 0028, South Africa
[b]Department of Mechanical Engineering, University of Cape Town,
Private Bag X3, Rondebosch 7701, South Africa
*E-mail: willemleroux@gmail.com

ABSTRACT

The successful design and operation of a small-scale solar thermal Brayton cycle depend on the successful understanding of the losses or irreversibilities in the system which are mainly due to heat transfer and fluid friction. The small-scale open solar thermal Brayton cycle uses air as working fluid which is heated in a cavity receiver which captures the solar radiation focused onto it from a parabolic concentrator. The goal of this work is to determine the optimum receiver tube diameter and counter-flow recuperator geometries of a small-scale open and direct solar thermal Brayton cycle with 4.8 m diameter parabolic dish, so that the net power output of the system is a maximum. In this work an updated receiver model is used. An open rectangular cavity receiver is used instead of a spherical receiver as was used in previous work. SolTrace is used to determine the solar heat flux rates on the receiver inner walls. The temperatures and net absorbed heat rates at different parts of the receiver tube are found by solving multiple equations using numerical methods. The model describing the heat loss rate from the recuperator to the environment is also updated in this work. Five different turbo-machines with different operating points are considered in this study. The results show the optimum geometries of the proposed system. It is shown that for the 4.8 m diameter solar dish with 0.25 x 0.25 m receiver aperture area, a receiver tube diameter of 83.3 mm will give the best results.

NOMENCLATURE

a	Receiver aperture side length or recuperator channel width, m
b	Recuperator channel height, m
A	Area, m^2
B	Constant
BSR	Blade speed ratio
c_1	Constant used in linear equation
c_2	Constant used in linear equation
c_{p0}	Constant pressure specific heat, J/kgK
Cr	Capacity ratio
D	Diameter, m
E	Constant
F	View factor
h	Heat transfer coefficient, W/m^2K
h	Specific enthalpy, J/kg
H	Recuperator height, m
k	Thermal conductivity, W/mK
k	Gas constant
L	Length of recuperator, m
m_1	Slope of linear equation
m_2	Slope of linear equation
$\dot{m}$	System mass flow rate, kg/s
M	Mass of recuperator, kg
MT	Micro-turbine number
n	Receiver tube section number along the length of tube
n	Number of recuperator flow channels in one direction
N	Number of tube sections
N	Speed of micro-turbine shaft, rpm
NTU	Number of transfer units
P	Pressure, Pa
r	Pressure ratio
R	Gas constant, J/kgK
R	Thermal resistance, K/W
$\dot{Q}$	Heat transfer rate, W
$\dot{Q}^*$	Rate of available solar heat at receiver cavity, W
$\dot{Q}_{loss}$	Rate of heat loss, W
$\dot{Q}_{net}$	Net heat transfer rate, W
$\dot{S}_{gen}$	Entropy generation rate, W/K
t	Thickness, m
T	Temperature, K
T^*	Apparent exergy-source sun temperature, K
U	Overall heat transfer coefficient, W/m^2K
w	Wind factor
$\dot{W}$	Power, W
V	Velocity, m/s
X	Dimensionless position
Z	Height, m

Greek Letters

ε	Emissivity of receiver
ε	Recuperator effectiveness
σ	Stefan-Boltzmann constant, W/m^{2}K
η	Efficiency
χ	Dimensionless external heat load
Θ	Dimensionless temperature difference

Subscripts

0	Initial inlet to receiver
1-11	Refer to Figure 1
ap	Aperture
bottom	At the bottom
c	Compressor
c	Based on the cold side
CF	Corrected flow
cond	Due to conduction
conv	Due to convection
h	Based on the hot side
in	At the inlet
ins	Insulation
int	Internal
inner	On the inside
l	Loss
max	Maximum
n	Tube section number
net	Net output
opt	Optimum
out	On the outside of the insulation
rad	Due to radiation
reg	Recuperator
s	Surface
side	At the side
solar	From solar as determined with SolTrace
t	Turbine
top	At the top
∞	Environment

INTRODUCTION

A small-scale solar thermal Brayton cycle experimental setup is underway at the University of Pretoria. It consists of a two-axis solar tracking structure on which a 4.8 m diameter aluminium parabolic dish is mounted to concentrate solar beam radiation onto a cavity receiver. The parabolic dish has a rim angle of 45 degrees and air is heated in the solar cavity receiver. The small-scale solar thermal Brayton cycle has the potential for high solar to mechanical conversion efficiency.

The open Brayton cycle uses air as working fluid, which makes this cycle very attractive for use in water-scarce countries. Research on the small-scale solar thermal Brayton cycle with thermodynamically optimised components has been published recently [1-5]. The open and direct solar thermal Brayton cycle is shown in Figure 1 [1]. The compressor increases the air pressure before the air is heated in the recuperator and solar receiver. The compressed and heated air expands in the turbine which produces rotational shaft power for the compressor and the load. The recuperator allows the hot exhaust air to preheat colder air before it enters the receiver.

Limiting factors to the performance of the solar thermal Brayton cycle include maximum receiver surface temperature and recuperator weight. It is often beneficial for the cycle to have a large recuperator, however the recuperator should be practical.

The method of total entropy generation minimisation is used to maximise the power output by simultaneously optimising the geometry variables of the components. The paper focuses on a holistic approach of optimising the system. Instead of optimising components individually, different components can be optimised together to reach a common goal, such as the maximum power output of the system. In this paper solutions are found for a specific sized system with concentrator diameter of 4.8 m. For this specific solar collector, five micro-turbines, three different receiver tube diameters and a number of differently sized recuperators are considered to determine which of these combinations would be the best for an experimental setup.

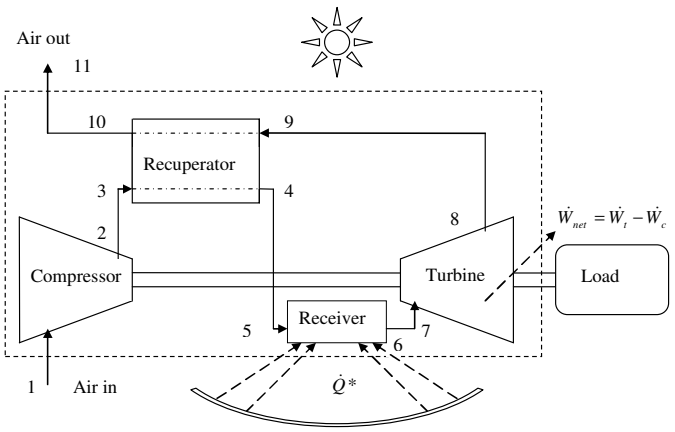

Figure 1 The open and direct solar thermal Brayton cycle.

SOLAR RECEIVER MODEL

The rectangular open cavity receiver model is shown in Figure 2 [5]. It consists of a stainless steel tube through which air travels. This rectangular or box solar cavity receiver is different to the half-spherical solar cavity receiver proposed in earlier work [1-3]. Reflected solar beam irradiance gets absorbed at the inner walls of the tube-formed cavity. The receiver is covered with insulation as shown in Figure 3 [5]. The heat loss from the receiver consists of convection, radiation and conduction and can be modelled by the Koenig and Marvin heat loss model [6] presented by Harris and Lenz [7]. For the rectangular receiver studied in this paper, the depth of the receiver is equal to 2a. The pressure drop through the receiver tube is calculated with the friction factor using the Colebrook equation [8].

There are many different variables at play to model the air temperature increase of the air running through such a receiver. These variables include concentrator shape, concentrator diameter, concentrator rim angle, concentrator reflectivity, concentrator optical error, tracking error, receiver aperture area, receiver material, receiver tube diameter, inlet temperature and mass flow rate through the receiver.

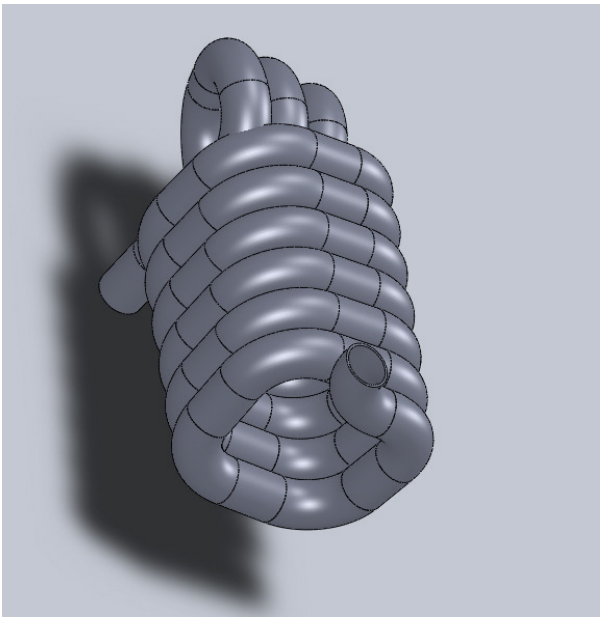

Figure 2 A rectangular open cavity solar receiver.

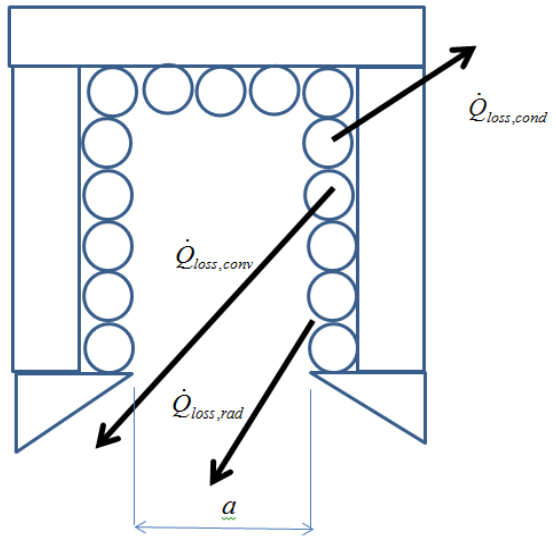

Figure 3 Heat loss from the open cavity solar receiver in section view.

Conduction heat loss

The conduction heat loss rate per area can be calculated with Equation (1) and (2) according to [5], by assuming an average wind speed of 2.5 m/s, which is the assumed average wind speed for Pretoria. Also note that an average surrounding temperature of 300 K and atmospheric pressure of 86.6 kPa is assumed throughout the paper.

$$\dot{Q}_{loss,cond,n} = \frac{A_n\left(T_{s,n} - T_\infty\right)}{R_{cond}} = \frac{\left(T_{s,n} - T_\infty\right)}{\left(1/h_{out}A_n + t_{ins}/k_{ins}A_n\right)} \quad (1)$$

where

$$\left(1/h_{out} + t_{ins}/k_{ins}\right) \approx 1.77 \quad (2)$$

An insulation thickness of t_{ins} = 0.1 m is assumed for the receiver walls. An average insulation conductivity of 0.061 W/mK at 550 °C is assumed [7]. The convection heat transfer coefficient on the outside of the insulation is determined by assuming a combination of natural convection and forced convection due to wind [5]. It can be assumed that the receiver will be operating at an average angle of 45° for most of its lifetime in Pretoria and also that the wind will mostly be either from the side or the back, since the dish would be shielding the receiver from wind. It is assumed that the effect of wind on the insulation is compared to forced convection on a flat plate for two sides of the receiver and the receiver top, and compared to a rectangular shape in forced convection for the other two sides of the receiver. In this paper, the heat loss from the receiver insulation due to radiation is neglected.

Radiation heat loss

The radiation heat loss rate can be calculated with Equation (3) [5]. This is the heat loss rate from the receiver aperture. The view factor is important when determining the temperature profile on the receiver tube. The view factors for this receiver is available from [5]. The receiver is built-up with a stainless steel tube. When calculating the temperature profile, the radiation heat loss and gain at each part of the inner wall is determined with the use of Equation (4).

$$\dot{Q}_{loss,n,rad} = \varepsilon\sigma A_{ap}\left(T_{s,n}^4 - T_\infty^4\right) \quad (3)$$

$$\dot{Q}_n = A_n\sum_{j=1}^{N} F_{n-j}\left(\varepsilon_n\sigma T_{s,n}^4 - \varepsilon_j\sigma T_{s,j}^4\right) \quad (4)$$

Convection heat loss

The convection heat loss rate from the open cavity receiver is determined according to [7]. According to [7], the convective heat loss coefficient for a cavity will depend on its shape, the orientation of the aperture with respect to the wind direction and the wind speed. Also, forced convection heat losses are quite sensitive to receiver tilt, wind speed and direction with respect to the aperture, and skirting or baffling placed around the aperture. According to [7], with no attempt to suppress forced convection, heat loss may be as much as four times the magnitude of natural convection heat loss in a 4.5 m/s wind blowing directly at the aperture. If a wind skirt is used, forced convection heat loss may be roughly twice the magnitude of the free convection heat loss. Forced convection heat loss decreases significantly when the wind direction differs from the direction in which the aperture is facing [7]. When the aperture is facing opposite to the wind direction, the heat loss is not much higher than for free convection heat loss. The convection heat loss rate from the open cavity receiver is determined from [7]:

$$\dot{Q}_{loss,conv,n} = wh_{inner}A_n\left(T_{s,n} - T_\infty\right) \quad (5)$$

where h_{inner}, the natural convection heat transfer coefficient, is determined as found in [5] and is equal to 2.75 and w, the wind effect constant is assumed equal to 2.

Optimum receiver aperture size

An optimum receiver aperture size of approximately 0.25 m x 0.25 m was identified by [5] and is used in this paper. By linearising the radiation heat loss terms and by using Gaussian elimination, a number of equations as shown in Equations (6) and (7), are solved simultaneously to determine the temperature profile ($T_{s,n}$) of the receiver tube and the net absorbed heat rate ($\dot{Q}_n$) at each tube section [5].

$$\dot{Q}_{net,n} = \frac{\left(T_{s,n} - \sum_{i=1}^{n-1} \left(\frac{\dot{Q}_{net,i}}{\dot{m} c_{p0}} \right) - T_{in,0} \right)}{\left(\frac{1}{hA_n} + \frac{1}{2\dot{m} c_{p0}} \right)} \tag{6}$$

and

$$\begin{aligned}
&\dot{Q}_{net,n} = \dot{Q}_{solar,n} - \dot{Q}_{loss,rad,n} - \dot{Q}_{loss,conv,n} - \dot{Q}_{loss,cond,n} \\
&\dot{Q}_{net,n} = \dot{Q}_{solar,n} - A_n \sum_{j=1}^{N} F_{n-j} \left(\varepsilon_n \sigma T_{s,n}^4 - \varepsilon_j \sigma T_{s,j}^4 \right) \\
&- A_n F_{n-\infty} \left(\varepsilon_n \sigma T_{s,n}^4 - \varepsilon_j \sigma T_{\infty}^4 \right) \\
&- h_n A_n \left(T_{s,n} - T_{\infty} \right) - A_n \left(T_{s,n} - T_{\infty} \right) / R_{cond} \\
&\dot{Q}_{net,n} = \dot{Q}_{solar,n} - A_n \varepsilon_n \sigma \left(m_1 T_{s,n} + c_1 \right) \\
&+ A_n \sum_{j=1}^{N} F_{n-j} \varepsilon_j \sigma \left(m_1 T_{s,j} + c_1 \right) - A_n \varepsilon_n \sigma F_{n-\infty} T_{\infty}^4 \\
&- A_n \left(m_2 T_{s,n} + c_2 \right) - \frac{A_n}{R_{cond}} \left(T_{s,n} - T_{\infty} \right)
\end{aligned} \tag{7}$$

Where $\dot{Q}_{solar,n}$ is determined with SolTrace, a solar ray-tracing software. SolTrace is recommended as a free and readily available plant performance code for solar receiver research [9,10]. A solar tracking error of 1° and an optical error of 10 mrad is used [5]. A solar dish reflectivity of 85% is assumed with a direct normal solar irradiance of 1 000 W/m^2.

RECUPERATOR MODEL

A counterflow plate-type recuperator is used as shown in Figure 4 [2]. The channels with length, L_{reg}, and aspect ratio, a/b are shown. The thickness of the material between the hot and cold stream, t, is 1 mm. The pressure drop through the recuperator is calculated with the friction factor for fully developed laminar flow or with the Colebrook equation [8], depending on the Reynolds number.

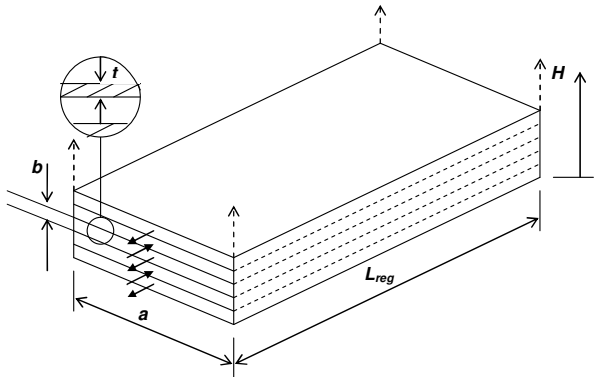

Figure 4 Recuperator geometry.

The recuperator efficiency can be calculated using the ε-NTU method. However in this paper an updated version of the ε-NTU method is used [11] which includes heat loss from the recuperator, since the recuperator is operating at a very high temperature and heat loss from the recuperator cannot be assumed negligible.

According to [11], the hot side and cold side efficiencies can be calculated with

$$\varepsilon_h = \begin{Bmatrix} 1 - \Theta_{X=1}, Cr_h < 1 \\ Cr_h \left(1 - \Theta_{X=1} \right), Cr_h > 1 \end{Bmatrix} \tag{8}$$

$$\varepsilon_c = \begin{Bmatrix} \frac{1 - \Theta_{X=0}}{Cr_h}, Cr_h < 1 \\ 1 - \Theta_{X=0}, Cr_h > 1 \end{Bmatrix} \tag{9}$$

where

$$\Theta_{X=0} = \frac{B + \left(\chi_h + Cr_h \chi_c \right) \left(1 - e^E \right)}{\left(Cr_h - 1 \right) \left(e^E - \frac{1}{Cr_h} \right)} \tag{10}$$

$$\Theta_{X=1} = NTU_h \left(\chi_c + \chi_h \right) + \frac{\left(\Theta_{X=0} - 1 \right)}{Cr_h} + 1 \tag{11}$$

and

$$B = \left(NTU_h \left(\chi_c + \chi_h \right) + \frac{Cr_h - 1}{Cr_h} \right) \left(Cr_h - 1 \right) \tag{12}$$

$$E = NTU_h \left(Cr_h - 1 \right) \tag{13}$$

$$Cr_h = \frac{\dot{m}_h c_{p0,h}}{\dot{m}_c c_{p0,c}} \tag{14}$$

$$NTU_h = \frac{UA}{\dot{m}_h c_{p0,h}} \tag{15}$$

$$\chi_h = \frac{\dot{Q}_{loss,h}}{UA\left(T_{h,in} - T_{c,in}\right)} \tag{16}$$

$$\chi_c = \frac{\dot{Q}_{loss,c}}{UA\left(T_{h,in} - T_{c,in}\right)} \tag{17}$$

In this paper, for the recuperator, the heat loss rate from the hot side and cold side of the recuperator is calculated with

$$\dot{Q}_{loss,h} = \frac{\dot{Q}_{loss,top,h}}{n} + \dot{Q}_{loss,side,h} \tag{18}$$

$$\dot{Q}_{loss,c} = \frac{\dot{Q}_{loss,bottom,c}}{n} + \dot{Q}_{loss,side,c} \tag{19}$$

where

$$\dot{Q}_{loss,top,h} = \frac{\left(T_9 + T_{10}\right)/2 - T_\infty}{R_{top,h}} \tag{20}$$

$$\dot{Q}_{loss,side,h} = \frac{\left(T_9 + T_{10}\right)/2 - T_\infty}{R_{side,h}} \tag{21}$$

$$\dot{Q}_{loss,bottom,c} = \frac{\left(T_3 + T_4\right)/2 - T_\infty}{R_{bottom,c}} \tag{22}$$

$$\dot{Q}_{loss,side,c} = \frac{\left(T_3 + T_4\right)/2 - T_\infty}{R_{side,c}} \tag{23}$$

and

$$R_{top,h} = \frac{1}{h_h aL} + \frac{t_{ins}}{k_{ins} aL} + \frac{1}{h_{out} aL} \tag{24}$$

$$R_{bottom,c} = \frac{1}{h_c aL} + \frac{t_{ins}}{k_{ins} aL} + \frac{1}{h_{out} aL} \tag{25}$$

$$R_{side,h} = \frac{1}{h_h bL} + \frac{t_{ins}}{k_{ins} bL} + \frac{1}{h_{out} bL} \tag{26}$$

$$R_{side,c} = \frac{1}{h_c bL} + \frac{t_{ins}}{k_{ins} bL} + \frac{1}{h_{out} bL} \tag{27}$$

TURBINE MODEL

A standard off-the-shelf micro-turbine from Honeywell [12] is used. Note that in this work, the geometry of the micro-turbine is fixed and is not optimised. When considering geometric optimisation of components, in a system using a turbo-machine, the compressor or turbine pressure ratio can be chosen as a parameter [13-15]. In this work, the turbine operating point (turbine corrected mass flow rate and turbine pressure ratio) is chosen. The turbine corrected mass flow rate and turbine pressure ratio can be modelled with the use of the turbine map, when considering experimental results for turbines and their mass flow rates [16]. Note that the turbine corrected mass flow rate is a function of the turbine pressure ratio. The turbine operating point is thus used as parameter in the objective function so that the maximum of the objective function can be found at different parameter values.

The compressor isentropic efficiency, compressor corrected mass flow rate, compressor pressure ratio and rotational speed are intrinsically coupled to each other and are available from the compressor map [12]. The compressor isentropic efficiency and shaft speed is obtained with interpolation. The compressor should operate within its compressor map range, otherwise flow surge or choking can occur. The turbine efficiency is determined from [4] by calculating the blade speed ratio [17-19] as

$$BSR = \frac{\frac{2\pi N}{60}\left(\frac{D_t}{2}\right)}{\left[2h_{in}\left(1 - r_t^{\frac{1-k}{k}}\right)\right]^{1/2}} \tag{28}$$

The turbine efficiency can be modelled as a parabolic function of the blade speed ratio [18]:

$$\eta_t = \eta_{t,\max}\left(1 - \left(\frac{BSR - 0.6}{0.6}\right)^2\right) \tag{29}$$

According to Guzzella and Onder [20], in automotive applications, typical values of the maximum turbine efficiency are $\eta_{t,\max} \approx 0.65$ - 0.75.

METHODOLOGY

The different combinations of 5 micro-turbines by Garrett [12], 3 different receiver tube diameters and 625 differently sized recuperators are used as parameters and variables to determine the net power output of the system. MATLAB [21] is used to determine the variables which will give the best results. The recuperator variables are the width of the recuperator channel, *a*, the height of a recuperator channel, *b*, the length of the recuperator, *L*, and the number of flow channels in one direction, *n*.

The basic structure of the MATLAB program is as follows, where *D* is the receiver tube diameter:

For *D* = 0.05, 0.0625 or 0.0833,
  For *MT* = 1:5,
    For the different operating points of each turbine,
      For 625 different recuperators,
      Find temperatures and pressures in the cycle with iteration

It is assumed that $T_8 = T_9$ and $P_8 = P_9$ (the recuperator and micro-turbine are close to each other), with reference to Figure 1. The system mass flow rate is equal to the actual turbine mass flow rate and is calculated with Eq. (30).

$$\dot{m}_t = \frac{\dot{m}_{tCF} \times P_7 / 14.7}{\sqrt{(T_7 + 460)/519}} \tag{30}$$

where P_7 is in psi and T_7 in degrees Fahrenheit respectively [12]. It is assumed that the pipe going to and from the receiver is 6 m long with 10 mm insulation thickness with 0.18 W/mK conduction heat transfer coefficient. The pressure drop for pipes with turbulent flow uses the friction factor from the Colebrook equation [8] for rough stainless steel. It is assumed that $T_2 = T_3$ and $P_2 = P_3$ (the recuperator and micro-turbine are close to each other). Note that T_1 = 300 K and $P_1 = P_{10} = P_{11}$ = 86 kPa (see Figure 1). The temperatures in the system are found using the isentropic efficiencies, recuperator efficiency and iteration.

For maximum net power output the total entropy generation rate is a minimum. The finite heat transfers and pressure drops in the compressor, turbine, recuperator, receiver and other tubes are identified as entropy generation mechanisms. When doing an exergy analysis for the system and assuming $V_1 = V_{11}$ and $Z_1 = Z_{11}$ (Figure 1), the objective function is assembled as shown in Eq. (31). The function to be maximised (the objective function), is $\dot{W}_{net}$ (the net power output). Eq. (32) shows the total entropy generation rate in terms of the temperatures and pressures (with reference to Figure 1). The entropy generation rate for each component is added and is shown in block brackets.

$$\dot{W}_{net} = -T_\infty \dot{S}_{gen,\text{int}} + \left(1 - \frac{T_\infty}{T^*}\right)\dot{Q}^* + \dot{m}c_{p0}(T_1 - T_{11}) - \dot{m}T_\infty c_{p0} \ln\left(\frac{T_1}{T_{11}}\right) \tag{31}$$

where

$$\begin{aligned}
\dot{S}_{gen,\text{int}} = {} & \left[-\dot{m}c_{p0}\ln(T_1/T_2) + \dot{m}R\ln(P_1/P_2)\right]_{compressor} \\
& + \left[\dot{Q}_l/T_\infty + \dot{m}c_{p0}\ln(T_3/T_2) - \dot{m}R\ln(P_3/P_2)\right]_{Duct23} \\
& + \left[\dot{m}c_{p0}\ln\left[\frac{T_{10}T_4}{T_9T_3}\left(\frac{P_{10}P_4}{P_9P_3}\right)^{-R/c_{p0}}\right] + \dot{Q}_l/T_\infty\right]_{recuperator} \\
& + \left[\dot{Q}_l/T_\infty + \dot{m}c_{p0}\ln(T_5/T_4) - \dot{m}R\ln(P_5/P_4)\right]_{Duct45} \\
& + \left[-\frac{\dot{Q}^*}{T^*} + \frac{\dot{Q}_{loss}}{T_\infty} + \dot{m}c_{p0}\ln(T_6/T_5) - \dot{m}R\ln(P_6/P_5)\right]_{receiver} \\
& + \left[\dot{Q}_l/T_\infty + \dot{m}c_{p0}\ln(T_7/T_6) - \dot{m}R\ln(P_7/P_6)\right]_{Duct67} \\
& + \left[-\dot{m}c_{p0}\ln(T_7/T_8) + \dot{m}R\ln(P_7/P_8)\right]_{turbine} \\
& + \left[\dot{Q}_l/T_\infty + \dot{m}c_{p0}\ln(T_9/T_8) - \dot{m}R\ln(P_9/P_8)\right]_{Duct89}
\end{aligned} \tag{32}$$

Note that $\dot{Q}^* - \dot{Q}_{loss} = \dot{Q}_{net}$. For comparison, the net power output is also calculated with the first law with a control volume around the micro-turbine and also around the system.

CONSTRAINTS

The one constraint on the system is the maximum receiver surface temperature which is constrained to 1 200 K. The second constraint is the recuperator total plate mass which is restricted to either 300 kg, 400 kg or 500 kg. The recuperator material is stainless steel.

RESULTS

In Figure 5 – Figure 9, it is shown that the maximum net power output of the system can be found when a large receiver tube diameter is used, for all 5 of the micro-turbines used. Note that each data point represents a maximum which is achieved using a unique optimised recuperator. Each data point is at a different turbine pressure ratio. Note that in these results the recuperator mass is restricted to 500 kg. Table 1 shows the results for MT = 5 with a receiver tube diameter of 0.0833 m (compare with Figure 9).

Table 1 Optimum recuperator geometries, maximum net power output, maximum receiver surface temperature and recuperator mass for MT = 5 and receiver tube diameter, D = 0.0833 m.

r_t	a (m)	b (m)	L (m)	n	$\dot{W}_{net,\max}$ (W)	$T_{s,max}$ (K)	Mass (kg)
1.688	0.15	0.005	1.5	15	946	1178	111.2
1.75	0.225	0.005	1.5	15	1168	1198	165.2
1.813	0.3	0.005	1.5	15	1353	1198	219.2
1.875	0.45	0.005	1.5	15	1575	1198	327.2
1.938	0.45	0.004	2.25	15	1808	1196	490
2	0.15	0.003	2.25	45	1848	1199	495.7
2.063	0.225	0.002	1.5	45	1991	1196	489.2
2.125	0.225	0.002	1.5	45	2058	1170	489.2
2.188	0.225	0.002	1.5	45	2110	1134	490.9
2.25	0.225	0.002	1.5	45	1714	1111	490.9
2.313	0.225	0.002	1.5	45	1662	1087	490.9
2.375	0.225	0.002	1.5	45	1577	1075	489.2
2.438	0.225	0.002	1.5	45	1571	1046	490.9

For each turbine pressure ratio shown in Table 1, a maximum net power output is given with the optimum recuperator geometries. The maximum receiver surface temperature and recuperator mass is given. Table 1 shows that a recuperator with a = 225 mm, b = 2.25 mm, L = 1.5 m and n = 45 is the best performing recuperator since it gave the highest maximum net power output. These optimum recuperator geometries were also found at most of the turbo-machines considered when a receiver tube diameter of 0.0833 m was used

and the recuperator mass was restricted to 500 kg. Also note that the maximum receiver surface temperature is restricted to 1 200 K.

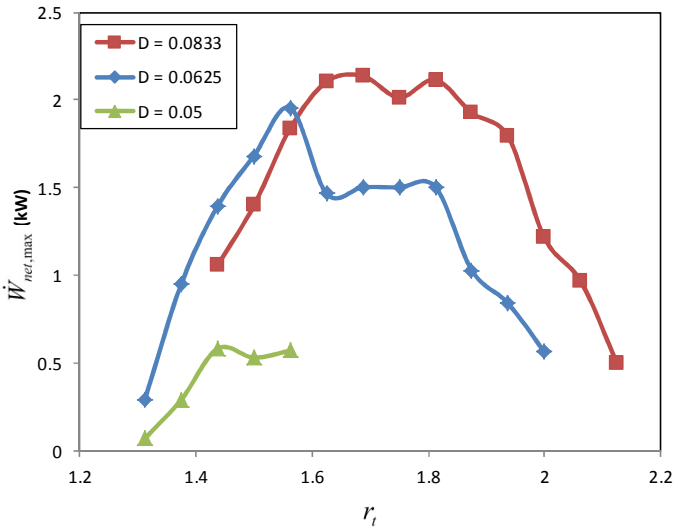

Figure 5 Maximum net power output of the system for $MT = 1$.

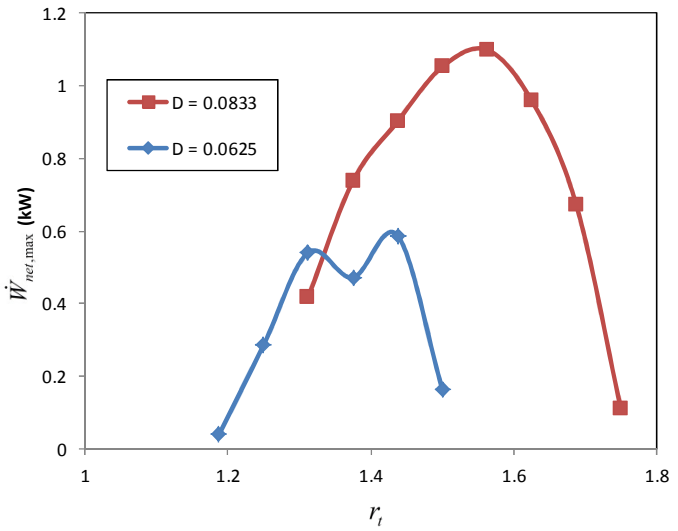

Figure 6 Maximum net power output of the system for $MT = 2$.

The larger the mass of the recuperator, the higher the net power output of the system as shown in Figure 10 and 11. When the recuperator mass is constrained to 400 kg, a recuperator with a = 150 mm, b = 2.25 mm, L = 1.5 m and n = 45 was found to be the most common optimum. When the recuperator mass is constrained to 300 kg, a recuperator with a = 150 mm, b = 2.25 mm, L = 1.5 m and n = 37.5 is best.

From Figures 12 and 13 it is shown that it is optimum for the maximum receiver tube surface temperature to decrease with increasing turbine pressure ratio and with decreasing receiver tube diameter.

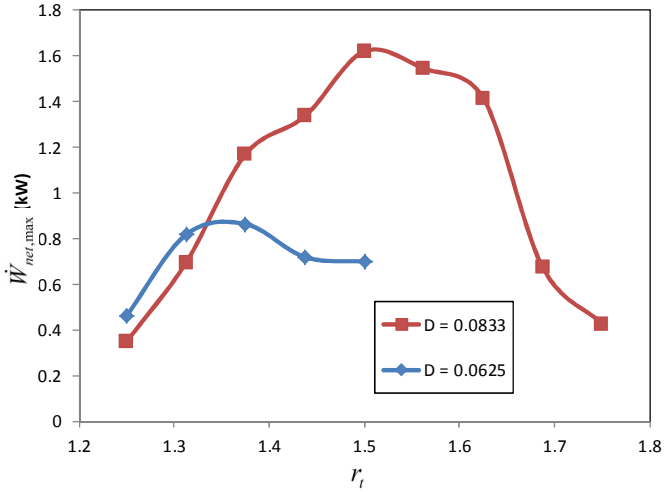

Figure 7 Maximum net power output of the system for $MT = 3$.

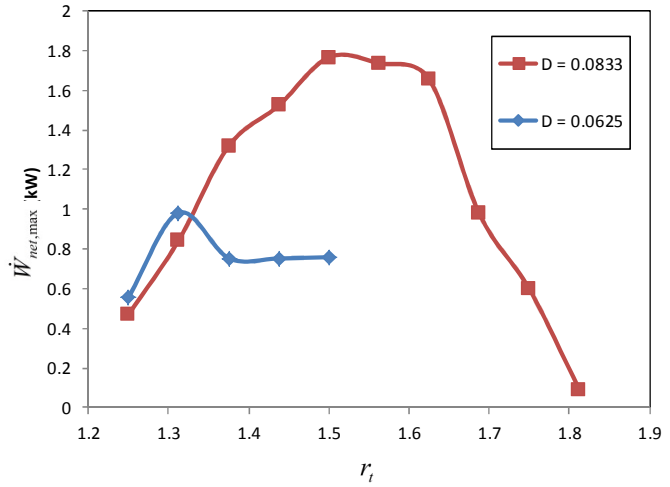

Figure 8 Maximum net power output of the system for $MT = 4$.

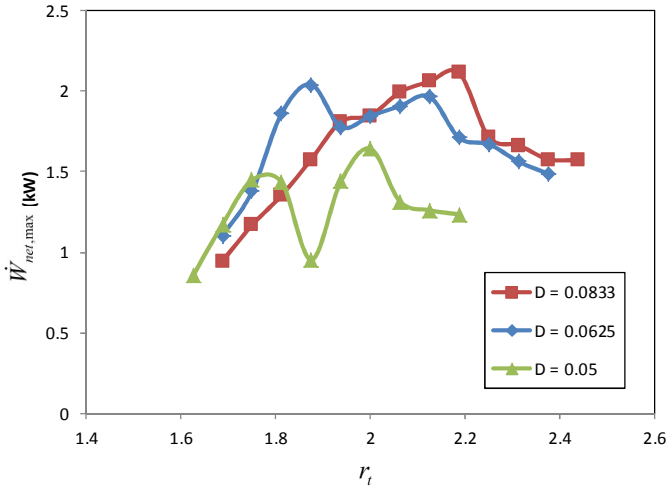

Figure 9 Maximum net power output of the system for $MT = 5$.

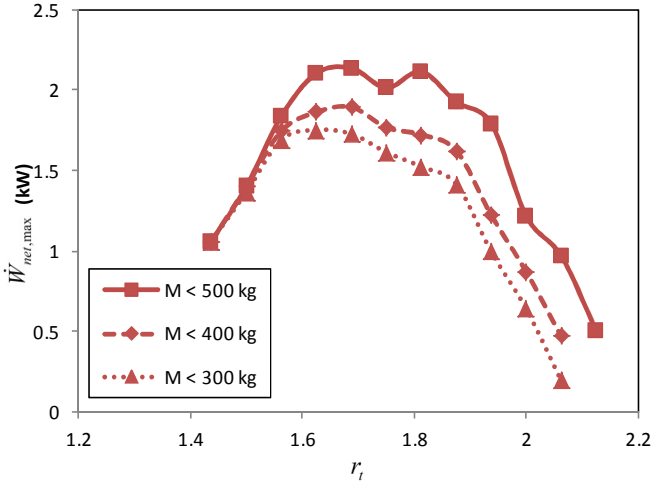

Figure 10 Maximum net power output of the system for $MT = 1$ with different recuperator mass constraints.

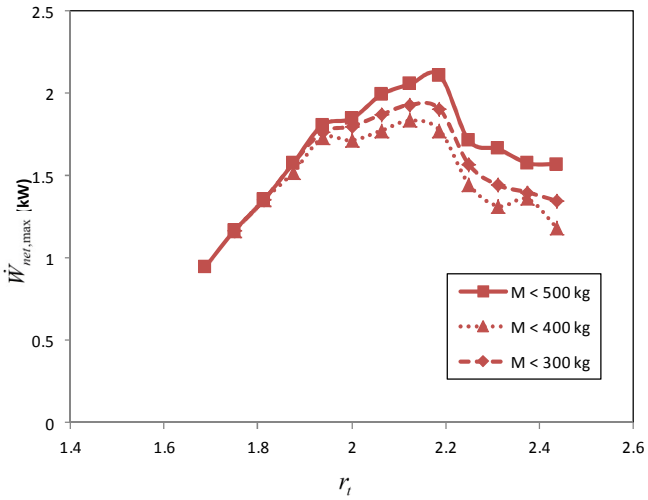

Figure 11 Maximum net power output of the system for $MT = 5$ with different recuperator mass constraints.

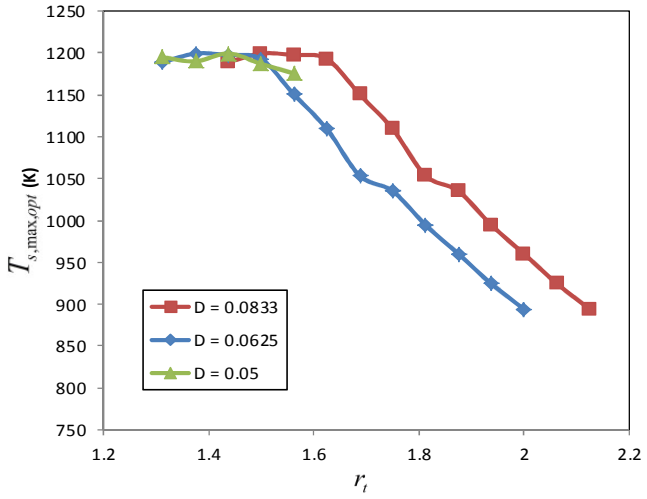

Figure 12 Optimum maximum receiver tube surface temperature at different operating temperatures for $MT = 1$.

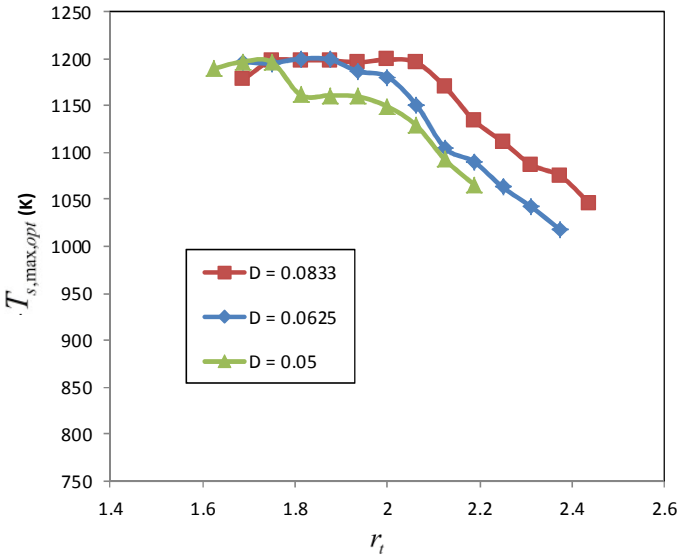

Figure 13 Optimum maximum receiver tube surface temperature at different operating temperatures for $MT = 5$.

CONCLUSION

A receiver and recuperator with thermal losses were optimised to perform in a small-scale solar thermal Brayton cycle. It was found that a 0.0833 m tube diameter should be sufficient for an experimental setup. This tube gives acceptable results when used with different turbo-machines. Even larger tube diameters can be studied for future work. It was found that a recuperator with a = 225 mm, b = 2.25 mm, L = 1.5 m and n = 45 gives the best results for the setup with recuperator mass constraint and receiver maximum surface temperature constraint. The larger the mass of the recuperator, the higher the power output of the system. At high turbine pressure ratios, the large receiver tube diameter has a higher surface temperature and it allows for higher net power output of the small-scale solar thermal Brayton cycle.

REFERENCES

[1] Le Roux, W.G., Bello-Ochende, T. and Meyer, J.P., 2011, Operating conditions of an open and direct solar thermal Brayton cycle with optimised cavity receiver and recuperator, *Energy* 36: pp. 6027-6036.

[2] Le Roux, W. G., Bello-Ochende, T. and Meyer, J.P., 2012, Thermodynamic optimisation of an integrated design of a small-scale solar thermal Brayton cycle, *International Journal of Energy Research*, 36: pp. 1088–1104.

[3] Le Roux, W.G., Bello-Ochende, T. and Meyer, J.P., 2012, Optimum performance of the small-scale open and direct solar thermal Brayton cycle at various environmental conditions and constraints, *Energy* 46, pp. 42 – 50.

[4] Le Roux, W.G., Bello-Ochende, T. and Meyer, J.P., 2013, A review on the thermodynamic optimisation and modelling of the solar thermal Brayton cycle, *Renewable and Sustainable Energy Reviews* 28, pp. 677–690.

[5] Le Roux, W.G., Bello-Ochende, T. and Meyer, J.P., 2014, The efficiency of an open cavity solar receiver for a small-scale solar thermal Brayton cycle, *Energy Conversion and Management* – Paper number: ECM-D-14-00336 (Submitted on 6 Feb 2014).

[6] McDonald, C.G., 1995, Heat loss from an open cavity, SAND95-2939, Sandia National Laboratories Albuquerque, New Mexico.
[7] Harris, J.A., Lenz, T.G., 1983, Thermal performance of solar concentrator/cavity receiver systems, *Solar Energy* 34 (2), pp. 135-142.
[8] Colebrook, C.F., 1939, Turbulent flow in pipes, with particular reference to the transition between the smooth and rough pipe laws, *Journal of the Institute of Civil Engineers London* 11, pp. 133-156.
[9] Ho, C.K., 2008. Software and Codes for Analysis of Concentrating Solar Power Technologies, Sandia Laboratory Report: SAND2008-8053.
[10] Bode SJ, Gauché P. Review of optical software for use in concentrated solar power systems. In: Proceedings of the Southern African Solar Energy Conference, SASEC, May, Stellenbosch, South Africa; 2012.
[11] Nellis, G.F. and Pfotenhauer, J.M., 2005, Effectiveness-NTU relationship for a counterflow heat exchanger subjected to an external heat transfer, *Journal of Heat Transfer* 127, pp. 1071 – 1073.
[12] Garrett, Garrett by Honeywell: turbochargers, intercoolers, upgrades, wastegates, blow-off valves, turbo-tutorials. Available at: http://www.TurboByGarrett.com; 2009 [accessed 26.04.2010].
[13] Snyman, J.A., 2009, Practical mathematical optimization, Pretoria: University of Pretoria.
[14] Wilson, D.G. and Korakianitis T., 1998, The design of high-efficiency turbomachinery and gas turbines, 2nd ed. New Jersey: Prentice Hall.
[15] Lidsky, L.M., Lanning, D.D., Staudt, J.E., Yan, X.L., Kaburaki, H., Mori, M., et al., 1991, A direct-cycle gas turbine power plant for near-term application: MGR-GT, *Energy* 16, pp.177-86.
[16] Zhuge, W., Zhang, Y., Zheng, X., Yang, M. and He, Y., 2009, Development of an advanced turbocharger simulation method for cycle simulation of turbocharged internal combustion engines. Proceedings of the Institution of Mechanical Engineers, Part D: Journal of Automobile Engineering 223: 661. doi:10.1243/09544070JAUTO975.
[17] Westin, F., 2005, Simulation of turbocharged SI-engines—with focus on the turbine. Doctoral thesis. KTH School of Industrial Engineering and Management, TRITA—MMK 2005:05. Stockholm: Royal Institute of Technology.
[18] Wahlström, J. and Eriksson, L., 2011, Modeling diesel engines with a variable-geometry turbocharger and exhaust gas recirculation by optimization of model parameters for capturing non-linear system dynamics. Proceedings of the Institution of Mechanical Engineers, Part D, Journal of Automobile Engineering 225 (July 7).
[19] Batteh, J.J. and Newman, C.E., 2008, Detailed simulation of turbocharged engines with Modelica, (March 3 and 4), The Modelica Association.
[20] Guzzella, L. and Onder, C.H., Introduction to modeling and control of internal combustion engine systems. second ed.. Berlin, Germany: Springer-Verlag; http://dx.doi.org/10.1007/978-3-642-10775-7.
[21] MATLAB version 7.6.0.324 Natick, Massachusetts: The MathWorks Inc., 2008.